Time-Resolved SAXS Study of Morphological Change in a Binary Blend of Poly(ϵ-caprolactone) and Polystyrene Oligomer

Shuichi Nojima,* Kazunori Kato, Mitsugu Ono, and Tamaichi Ashida

Department of Biotechnology, School of Engineering, Nagoya University, Nagoya 464-01, Japan

Received July 22, 1991; Revised Manuscript Received October 22, 1991

ABSTRACT: The process of morphology formation in a binary blend of poly(ϵ-caprolactone) (PCL) and polystyrene oligomer (PSO) has been observed at various temperatures and compositions by small-angle X-ray scattering (SAXS) employing synchrotron radiation. A strong scattering at smaller angle was observed during the morphology formation in addition to the intensity maximum arising from the crystalline region consisting of the alternate stacks of lamellae and amorphous layers. These SAXS curves indicate a possible coexistence of the crystalline region and the amorphous region (rich in PSO) throughout the morphology formation in the blend. The time dependence of parameters characterizing the crystalline region is similar in features to that of the crystallization of homopolymers, suggesting that the rate of morphology formation is substantially controlled by the crystallization of PCL. The analysis based on the combination of the paracrystalline lattice model developed by Hosemann and the two-phase model by Debye and Bueche shows that phase separation takes place simultaneously with crystallization of PCL on the morphology formation to determine the details of the complicated morphology in the present system.

Introduction

It has been well-known that in binary compatible crystalline/amorphous polymer blends the amorphous component is expelled from lamellar crystals during crystallization and eventually accommodated into the amorphous layer between lamellae. As a result, an increase of long spacing, an alternating distance of lamellae and amorphous layers, can be observed by small-angle X-ray scattering (SAXS) with increasing amorphous fraction in the system.[1] It is manifested with a number of polymer blend systems, such as poly(ϵ-caprolactone) (PCL)/poly(vinyl chloride) (PVC),[2-4] poly(vinylidene fluoride) (PVF_2)/poly(methyl methacrylate) (PMMA),[5,6] and poly(ethylene oxide) (PEO)/PMMA systems.[7,8] The process of polymer crystallization from the homopolymer melt or compatible blends has recently been investigated by SAXS with synchrotron radiation.[4,9-17] The results show that blending amorphous polymers yields a significant reduction of the crystallization rate but main features of crystallization are similar to those of the homopolymer crystallization.

In binary polymer blends, phase separation between components may intervene in the morphology formation when the constituent polymer crystallizes, and a complicated morphology will be formed by a cooperative effect of phase separation and crystallization.[18-24] We have recently investigated the morphology of such a system, the poly(ϵ-caprolactone) and polystyrene oligomer (PSO) system, at various PCL compositions (ϕ_{PCL}) and crystallization temperatures (T_c) by SAXS and differential scanning calorimetry (DSC).[21,22] This system has a UCST-type coexistence curve with the critical composition in the vicinity of $\phi_{PCL} \sim 0.2$, and PCL crystallizes below 60 °C in the blend. Competition is, therefore, expected between the phase separation and PCL crystallization during the morphology formation. We have proposed a tentative phase diagram of this system and discussed that the phase separation should take place simultaneously with the crystallization of PCL even for the samples quenched outside the binodals.[22] As a result, the final morphology is a mosaic structure consisting of the amorphous region rich in PSO and the crystalline region with lamellae and amorphous layers (Figure 1). The amorphous layer in the crystalline region may accommodate a limited amount of PSO. The phase diagram also successfully explains the T_c dependence of complicated spherulites in the PCL/PSO system recently observed by Tanaka and Nishi.[23,24]

In the present study, the process of morphology formation in the PCL/PSO system at various ϕ_{PCL} and T_c values has been investigated by SAXS with synchrotron radiation. The SAXS curves are compared with those from the pure PCL, and the effect of blending PSO is elucidated as a function of T_c and ϕ_{PCL}. Next, it is demonstrated that phase separation takes place simultaneously with the crystallization of PCL from the time-sliced SAXS curves during the morphology formation. The results are interpreted with a combination of the paracrystalline lattice model developed by Hosemann[25] and the two-phase model developed by Debye and Bueche.[26] The parameters characterizing the morphology, such as long spacing and correlation length, are evaluated as a function of time at each T_c and ϕ_{PCL}.

Experimental Section

1. Materials and Sample Preparation. The poly(ϵ-caprolactone) (PCL) used in this study was supplied by Scientific Polymer Products Inc. and was fractionated with a benzene/*n*-heptane system. The weight-average molecular weight M_w determined by gel permeation chromatography was 13 700, and the ratio of M_w to number-average molecular weight M_n, M_w/M_n, was 1.44. Polystyrene oligomer (PSO) was purchased from Tosoh Corp., and M_w and M_w/M_n were stated to be 950 and 1.13, respectively.

The solvent-casting method was employed to prepare blends with various ϕ_{PCL} values ranging from 0.60 to 1.0. PCL and PSO were dissolved in a common solvent, benzene, at a polymer concentration less than 15%. The solution was cast on a glass plate, and the solvent was evaporated under vacuum at 80 °C for more than 40 h.

2. Small-Angle X-ray Scattering (SAXS) Measurement with Synchrotron Radiation.[27] The process of morphology formation in the blends was observed by small-angle X-ray scattering (SAXS) with synchrotron radiation. The experiment was carried out at National Laboratory for High Energy Physics, Tsukuba, Japan (Photon Factory), with small-angle X-ray equipment for solution (SAXES) installed at beam line BL-10C.

The storage ring was operated at an energy level of 2.5 GeV with the ring current of 250–300 mA during the period of 12 or 24 h. The SAXES employs a *point* focusing optics with a double

0024-9297/92/2225-1922$03.00/0

flat monochromator followed by a bent cylindrical mirror. The incident beam intensity (with wavelength λ = 0.1488 nm) was monitored by an ionization chamber for the correction of minor decrease of the primary beam intensity during the measurement. The scattered intensity was detected with a one-dimensional position sensitive proportional counter (PSPC) with 512 channels, and the distance between the sample and the PSPC was about 2000 mm. The geometry was further checked by a chicken tendon collagen, which gives a set of sharp diffractions corresponding to 65.3 nm. Details of the optics and instrumentation are described elsewhere.[28]

The temperature control of the sample holder was achieved by circulating water of constant temperature by which the temperature fluctuation was achieved within the range of 0.2 °C throughout the experiment. The morphology formation was started by dropping the water temperature from the homogeneous state of the sample (ca. 65 °C) to T_c, and it took less than 1 min for the sample to reach T_c. The SAXS intensity was collected as the sum of the scattered intensity during the period of 10 or 20 s from the beginning of temperature drop, and the measurement was continued until the integrated intensity ceased to change.

The SAXS intensity measured was corrected for the decrease of the ring current, background scattering, and finally Lorentz factor. Since the optics of SAXES is *point* focusing, the intensity was not corrected for the smearing effect by the finite cross section of the primary beam. The Lorentz-corrected SAXS intensity against s (=2 sin θ/λ, 2θ is the scattering angle) was obtained as a function of time t after the temperature has dropped to T_c.

3. Analysis of Time-Resolved SAXS Curves. The SAXS curve obtained during morphology formation is the superposition of the two scattered intensities: one having a peak at $s \sim 0.06$ nm^{-1} and arising from the crystalline region consisting of the alternating stacks of lamellae and amorphous layers, and another increasing intensity as $s \to 0$, suggesting its peak is probably located at $s = 0$. The intensity from the crystalline region is successfully approximated in the previous papers[21,22] by the paracrystalline lattice theory developed by Hosemann.[25] The Lorentz-corrected scattered intensity $s^2I(s)$ obtained at t is given by

$$s^2I(s) \propto V_c(t)\langle(\rho_l - \rho_a)^2\rangle \times \frac{\left\{Re\left(N\frac{(1-f_c)(1-f_a)}{1-f_cf_a}\right) + Re\left[f_a\left(\frac{1-f_c}{1-f_cf_a}\right)^2[1-(f_cf_a)^N]\right]\right\}}{2\pi^2s^2} \quad (1)$$

where ρ_l and ρ_a represent the electron density of the lamella and amorphous layer, respectively, and are time-independent if we ignore the minor variation in composition of the amorphous layer. $V_c(t)$ is the volume fraction of the crystalline region in the blend at t, N is the mean number of the repeating unit of the lamella and amorphous layer within a crystalline region, and f_c and f_a are the Fourier transforms of the thickness distribution functions $h_c(x)$ and $h_a(x)$ of the lamella (with mean thickness l_c and distribution β_c) and amorphous layer (l_a and β_a), respectively, given by

$$h_c(x) = \frac{1}{\beta_c(2\pi)^{1/2}}\exp\left(-\frac{(x-l_c)^2}{2\beta_c^2}\right) \quad (2)$$

$$h_a(x) = \frac{1}{\beta_a(2\pi)^{1/2}}\exp\left(-\frac{(x-l_a)^2}{2\beta_a^2}\right) \quad (3)$$

The SAXS peak intensity $(s^2I(s))_{max}$ at t is proportional to $V_c(t)$ if we assume that the parameters characterizing the crystalline region do not change during the morphology formation, so that t dependence of $V_c(t)$ is simply evaluated from the SAXS intensity maximum. The intensity at smaller angle arises from the inhomogeneity of the system. This inhomogeneity will not be a phase-separated structure such as a modulated structure due to the spinodal decomposition[29] but the two-phase structure (similar to the structure at the late stage of phase separation) illustrated in Figure 1, because the process of morphology formation is essentially controlled by the crystallization of PCL, as is found later, and the coagulation rate of the amorphous phase is expected to be extremely large.[23,24] Therefore, it is reasonable that the morphology during the phase transition is approximated by the two-phase model, which is previously used for the final morphology of the present PCL/PSO system.[21,22] The SAXS intensity $I(s)$ during the morphology formation is described by

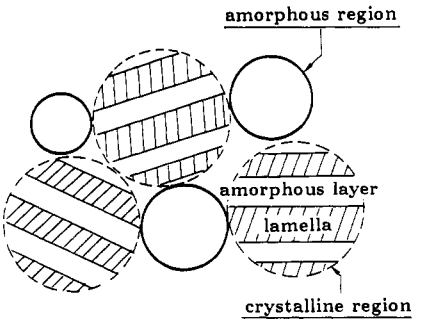

Figure 1. Schematic illustration proposed in our previous paper[22] showing the two-phase structure consisting of the crystalline and amorphous regions. The crystalline region comprises alternate stacks of lamellae and amorphous layers. The amorphous region is mainly composed of PSO. The proportion of this two-phase structure in the system increases with increasing time from the beginning of morphology formation.

$$I(s) \propto \frac{V(t)\langle(\rho'_a - \rho'_c)^2\rangle\xi^3}{(1 + 4\pi^2s^2\xi^2)^2} \quad (4)$$

where ξ is known as a correlation distance and defines the size of heterogeneity.[2] ρ'_c and ρ'_a represent the average electron density of the amorphous and crystalline regions and are time-independent. $V(t)$ is expressed as[2]

$$V(t) = \psi(t)(1-\psi(t))(V_c(t) + V_a(t)) \quad (5)$$

where $V_a(t)$ is the volume fraction of the amorphous region in the blend at t and $\psi(t)$ is the volume fraction of the crystalline region in the two-phase structure (i.e., $V_c(t)/(V_c(t) + V_a(t))$). The plot of $1/(I(s))^{1/2}$ against s^2 should be linear at smaller s, from which parameters ξ and $V(t)\langle(\rho'_a - \rho'_c)^2\rangle$ can be evaluated. Next, we consider the parameter $\vartheta(t)$ defined by

$$\vartheta(t) = V(t)/V_c(t) \quad (6)$$

$\vartheta(t)$ is equal to $1-\psi(t)$ and represents the volume fraction of the amorphous region in the two-phase structure. The SAXS measurement in the present study provides *relative* intensity, so that the value proportional to $\vartheta(t)$ is evaluated through eqs 1–6 instead of exact $\vartheta(t)$. The t dependence of $\vartheta(t)$ as well as ξ should give important information about the morphological change. We are especially interested in whether the two-phase structure illustrated in Figure 1 appears from the beginning of the morphology formation or whether the crystalline region (with lamellae and amorphous layers) appears first followed by the formation of the amorphous domain.

Results

The present PCL/PSO blend has a UCST-type coexistence curve with the critical composition in the vicinity of ϕ_{PCL} = 0.2, and PCL crystallizes below 60 °C in the blend.[21] From the phase diagram (binodals and melting temperature of PCL) of this system, all blends investigated ($0.6 \le \phi_{PCL} \le 1.0$) are homogeneous at above the melting temperature of PCL (~60 °C), and the morphological change was observed at temperatures ranging from 30.0 to 42.5 °C, where a complicated morphology is expected by a cooperative effect of liquid–liquid phase separation and crystallization. In our previous paper,[22] the final morphology was proposed to be a mosaic structure consisting of the crystalline region (made up of the alternate stacks of lamellae and amorphous layers) and the amorphous region with a PSO-rich composition (Figure 1). We discussed on the basis of the phase diagram that

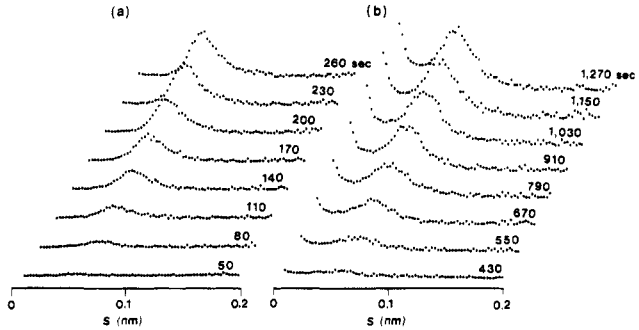

Figure 2. Time-resolved SAXS profiles during morphology formation at 40 °C for the blend with ϕ_{PCL} = 1.0 (a) and 0.6 (b). The SAXS intensity is corrected for the Lorentz factor. The numerals in the figure represent time from the beginning of morphology formation. Some of the data are omitted for the purpose of clarity.

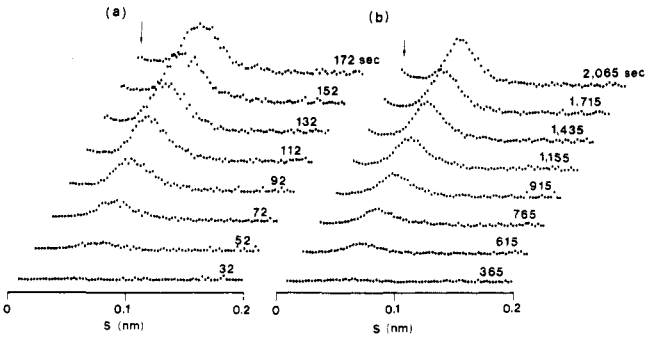

Figure 3. Time-resolved SAXS profiles during morphology formation for the blend with ϕ_{PCL} = 0.8 at T_c = 30.0 (a) and 42.5 °C (b).

liquid–liquid phase separation should take place simultaneously with crystallization; that is, the amorphous region appears at the beginning of the morphology formation and continues to increase. This means that the volume fraction of the amorphous region in the two-phase structure is constant throughout the morphology formation and the proportion of this mosaic structure increases with increasing t.

1. Time-Resolved SAXS Curves. Figure 2 shows the time-resolved SAXS curves corrected for the Lorentz factor from the blends with ϕ_{PCL} = 1.0 (a) and 0.6 (b) at T_c = 40 °C. In Figure 2a, the scattering maximum arising from the crystalline region appears at $s \sim 0.07$ nm^{-1} and grows with increasing time t after a short period of induction time. The growth of the scattering maximum is considered as a result of the increase of the crystalline region, as observed in the crystallization of many homopolymers.[4,12-17] The scattering curves of Figure 2b for the blend with ϕ_{PCL} = 0.6, on the other hand, have an increasing intensity toward smaller angle in addition to the intensity maximum at $s \sim 0.06$ nm^{-1} arising from the crystalline region. The SAXS intensity at smaller angle, which is increasing in intensity with t, could be observed on the final morphology of this system in the previous paper[22] and is attributed to a mosaic structure consisting of the crystalline and amorphous regions; i.e., an average electron-density difference between two regions makes the scattered intensity at smaller angle. This scattered intensity was successfully analyzed by means of the Debye–Bueche relation,[26] usually used for systems possessing a two-phase structure. The quantitative analysis of the time-resolved SAXS curves will appear in a following section.

Figure 3 shows the time-resolved SAXS curves from the blend with ϕ_{PCL} = 0.8 at T_c = 30.0 (a) and 42.5 °C (b). Both SAXS curves have a faint scattered intensity at

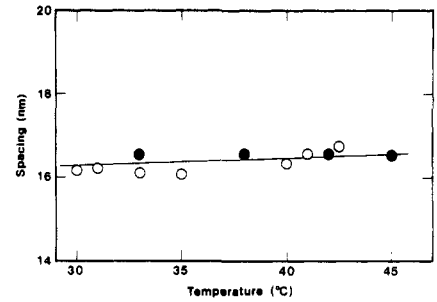

Figure 4. Final long spacing plotted against T_c for the blend with ϕ_{PCL} = 0.8. The open circle represents the present data obtained at the SAXES facility with synchrotron radiation, and the solid symbol shows the data previously obtained after the SAXS intensity with the Kratky camera was desmeared[30] for the same blend.[22]

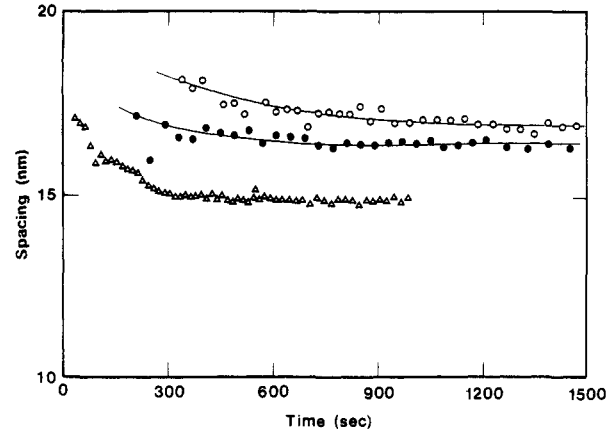

Figure 5. Long spacing, evaluated from the angular position of the intensity maximum, plotted against time for the blends crystallized at T_c = 40 °C with ϕ_{PCL} = 1.0 (△), 0.8 (●), and 0.6 (○).

smaller angle (indicated by arrow), and this scattered intensity grows slightly with decreasing T_c values. The difference in phase relations at different temperatures is not large, so that the resultant SAXS curve does not have a large difference in its shape. The other characteristic in Figure 3 is that the morphology completion takes a very long time at higher T_c, and no sign of phase separation (or scattered intensity at smaller angle) appears until the crystallization starts (or scattered peak appears at a finite angle). The extended process of crystallization with increasing T_c values can be usually found in the homopolymer crystallization, such as polyethylene[14-17] and poly(ε-caprolactone),[4] using SAXS with synchrotron radiation.

Before the time-resolved SAXS curves can be quantitatively analyzed, it is necessary to check the compatibility in scattering angle of the present results with that obtained previously with an Kratky camera.[22] Figure 4 shows the T_c dependence of the final long spacing for the blend with ϕ_{PCL} = 0.8, where results obtained by both the Kratky camera and the SAXES facility with synchrotron radiation coincide and no systematical error could be detected. A similar result also could be found for the ϕ_{PCL} dependence of the long spacing between both apparatus.

2. Time Dependence of SAXS Curves. Figure 5 shows the time dependence of long spacing L, a repeating distance of the lamella and amorphous layer, evaluated from the angular position of the maximum intensity of the SAXS curve for the blend with ϕ_{PCL} = 1.0 (pure PCL), 0.8, and 0.6 at T_c = 40 °C. The final L changes greatly in the range $0.8 \leq \phi_{PCL} \leq 1.0$ but changes only slightly or is almost constant in the range $\phi_{PCL} < 0.8$. The other

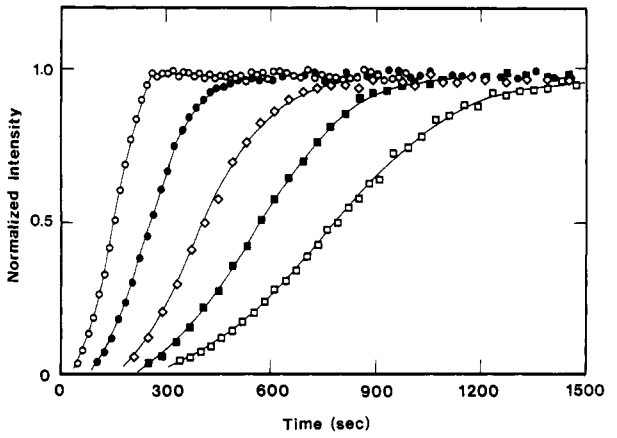

Figure 6. Normalized intensity maximum plotted against time for the blend crystallized at T_c = 40 °C with ϕ_{PCL} = 1.0 (○), 0.9 (●), 0.8 (◇), 0.7 (■), and 0.6 (□).

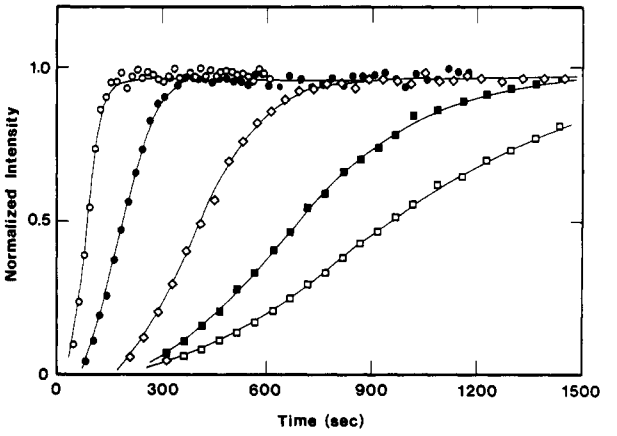

Figure 7. Normalized intensity maximum plotted against t for the blend with ϕ_{PCL} = 0.8 crystallized at T_c = 30.0 (○), 35.0 (●), 39.5 (◇), 41.0 (■), and 42.5 °C (□).

characteristic in Figure 5 is a large decrease of L at the early stage of morphology formation, especially remarkable in the pure PCL. This decrease was widely observed in the crystallization of homopolymers and is attributed to the rearrangement of bent lamellae appearing in the beginning of crystallization[9] or the thickening and/or thinning of lamellae during crystallization.[13] In the blends, on the other hand, this decrease is insignificant and difficult to distinguish from the experimental error. The lesser regularity of the lamellar structure in the blend, which is conveniently expressed in terms of N in eq 1 and decreasing N was demonstrated with decreasing ϕ_{PCL} values in our previous paper,[22] is responsible for the ambiguous decrease of L. The T_c dependence of L measured for the blend with ϕ_{PCL} = 0.8 in the range 30.0 ≤ T_c ≤ 42.5 °C, on the other hand, is negligibly small, and the decrease of L at the early stage of morphology formation was not clear for every T_c measured.

Figure 6 shows the time dependence of the normalized intensity maximum, i.e., peak intensity divided by the final intensity, for the blends with ϕ_{PCL} = 1.0, 0.9, 0.8, 0.7, and 0.6 at T_c = 40 °C, and Figure 7 shows that for the blend with ϕ_{PCL} = 0.8 at T_c = 30.0, 35.0, 39.5, 41.0, and 42.5 °C. These figures express the growth features of the crystalline region in the blend at each T_c and ϕ_{PCL}. The growing rate is slower with decreasing ϕ_{PCL} and with increasing T_c, which is qualitatively similar to the previous result with a compatible PCL/poly(vinyl chloride) blend.[4] The half-time of crystallization, $t_{1/2}$, i.e., the time necessary to reach the half-value at the angular position of the maximum intensity, is considered to be a measure for the

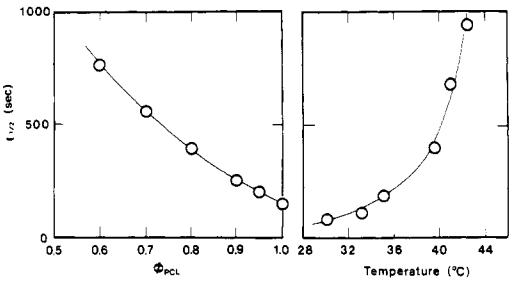

Figure 8. Half-time necessary to reach the final value at the angular position of the intensity maximum, $t_{1/2}$, plotted against ϕ_{PCL} at T_c = 40 °C (left) and against T_c for the blend with ϕ_{PCL} = 0.8 (right).

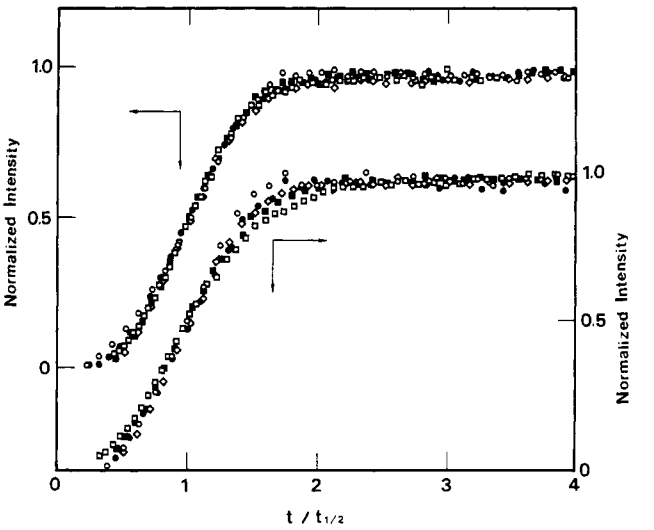

Figure 9. Normalized intensity maximum plotted against reduced time, $t/t_{1/2}$. In the upper curve, the data are obtained from the blends crystallized at 40 °C with ϕ_{PCL} = 1.0 (○), 0.9 (●), 0.8 (◇), 0.7 (■), and 0.6 (□). In the lower curve, the data points are from the blend with ϕ_{PCL} = 0.8 crystallized at T_c = 30.0 (○), 35.0 (●), 39.5 (◇), 41.0 (■), and 42.5 °C (□).

growth rate of the crystalline region and is plotted in Figure 8 against ϕ_{PCL} and T_c. $t_{1/2}$ increases remarkably with decreasing ϕ_{PCL} and increasing T_c, suggesting that blending the amorphous polymer has the effect of decreasing significantly the crystallization rate similar to increasing T_c.

To investigate quantitatively the effect of the amorphous polymer on morphology formation, the normalized intensity maximum is plotted against reduced time, $t/t_{1/2}$, in Figure 9 for different ϕ_{PCL} values at T_c = 40 °C (upper curve), together with the data at different T_c for the blend with ϕ_{PCL} = 0.8 (lower curve). Although the t dependence of the intensity maximum shows different curves in Figure 6 according to ϕ_{PCL}, they coincide with each other and make one master curve in Figure 9. This means that the overall feature of morphology formation in the blend, where crystallization and liquid–liquid phase separation may occur cooperatively, is the same as that of the pure crystalline polymer, where the crystallization is the only factor to form the morphology. Therefore, the crystallization of PCL controls the whole rate of morphology formation in the blend, because if liquid–liquid phase separation controls the process, the time dependence of the intensity maximum should be quite different from that of the pure PCL and a completely different mechanism for the morphology formation, for example, spinodal decomposition, will control the system.[29] The above results, of course, do not mean that the details of the morphology are determined by the crystallization of PCL.

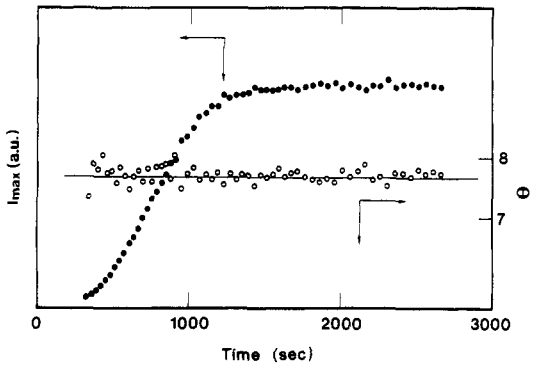

Figure 10. Intensity maximum $(s^2I)_{max}$ (●) and $\vartheta(t)$ (○) plotted against time for the blend with $\phi_{PCL} = 0.6$ at $T_c = 40.0$ °C. $\vartheta(t)$ is almost constant throughout morphology formation within the experimental error.

Rather, it is shown in the next section that the details of the morphology are determined by a cooperative effect of liquid–liquid phase separation and crystallization. The normalized intensity maximum at different T_c values is also successfully scaled by the reduced time (lower curve in Figure 9), suggesting that the effect of rising T_c is the same as that of blending the amorphous polymer as far as the growth rate of the morphology is concerned.

3. Analysis by Models. In our previous paper,[22] the structure within the crystalline region was successfully approximated by the paracrystalline lattice model proposed by Hosemann[25] with a correction of the boundary profile between the lamella and amorphous layer,[31] and the scattered intensity from the inhomogeneity (two-phase structure) was also expressed according to the model of Debye and Bueche.[26] This means that the interference effect of scattered intensity is insignificant even if it exists between the two-phase structure and the crystalline region. Figure 10 shows the t dependence of $\vartheta(t)$ for the blend with $\phi_{PCL} = 0.6$ at $T_c = 40.0$ °C, together with the plot of the intensity maximum arising from the crystalline region (proportional to $V_c(t)$). $V_c(t)$ and also $V(t)$ increase abruptly with increasing t and eventually level off at a constant value, indicating that with increasing t the crystalline region, amorphous region, and therefore two-phase structure appear, grow, and prevail in the system. The value of $\vartheta(t)$, on the other hand, is almost constant throughout the morphology formation. Especially at the early stage, in spite of the dramatic increase of the intensity maximum, $\vartheta(t)$ remains constant, although the data points are somewhat scattered because of the inadequacy of the scattered intensity. This constancy of $\vartheta(t)$ means that on the morphology formation the two-phase structure grows directly from the homogeneous melt of PCL and PSO, and amorphous regions (and also crystalline regions) appear with a constant proportion in the two-phase structure. Figure 10 does not support the usual concept about the morphology formation in compatible crystalline/amorphous blend systems, where the crystallization occurs first and the amorphous component ejected from the lamellar crystal is accommodated into the amorphous layer between lamellae, and eventually a new amorphous domain appears by the phase separation at this amorphous layer if the layer becomes thermodynamically unstable. Figure 10, on the other hand, suggests that in the present PCL/PSO system the morphology is formed simultaneously by a cooperative effect of liquid–liquid phase separation and PCL crystallization.

Figure 11 shows the t dependence of the correlation length ξ for the blend with $\phi_{PCL} = 0.6$ at $T_c = 39.5$ °C evaluated from eq 4. ξ is almost constant as well as $\vartheta(t)$

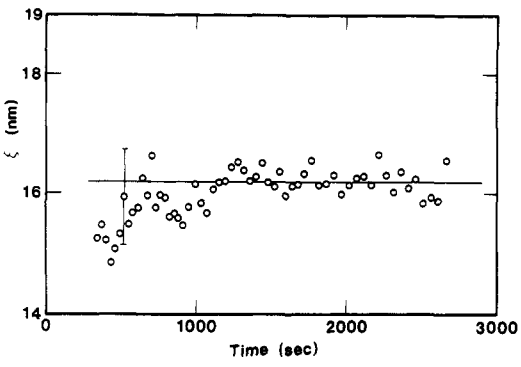

Figure 11. Correlation length, ξ, estimated from the Debye–Bueche relation (eq 4), plotted against time for the blend with $\phi_{PCL} = 0.6$ at $T_c = 40.0$ °C.

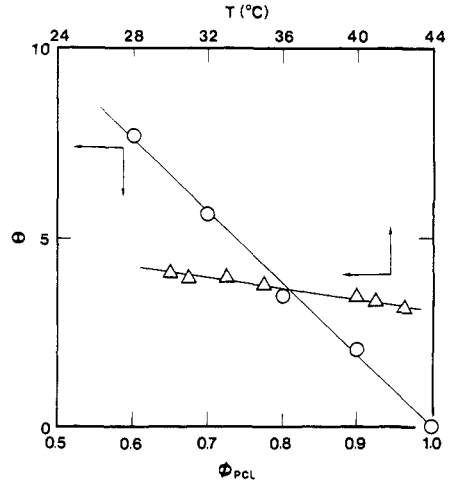

Figure 12. $\vartheta(\infty)$, evaluated from eq 6, plotted against T_c for the blend with $\phi_{PCL} = 0.8$ (△) and against ϕ_{PCL} at $T_c = 40$ °C (○).

irrespective of t, suggesting that the main feature of the two-phase structure, i.e., the interrelation between crystalline and amorphous regions, does not substantially change throughout the morphology formation and supporting the morphology formation by the cooperative effect of liquid–liquid phase separation and crystallization. The constancy of ξ could be derived at every condition studied.

Figure 12 shows the T_c and ϕ_{PCL} dependences of $\vartheta(t)$ evaluated by eq 6. Both $V_c(t)$ and $V(t)$ in eq 6 include the possible fluctuation in intensity or the occasional difference of the equipment as well as the morphological contribution, so that they cannot be directly compared each other. In the evaluation of $\vartheta(t)$, on the other hand, the accidental factors cancel out and $\vartheta(t)$ can directly be compared. $\vartheta(t)$ decreases remarkably with increasing ϕ_{PCL}, while it decreases slightly with increasing T_c. The change of $\vartheta(t)$ between $\phi_{PCL} = 1.0$ and 0.6 is about 10 times larger than the change between $T_c = 30.0$ and 42.5 °C. These changes should reflect the phase diagram of this system and can qualitatively be explained on the basis of the phase diagram of this system (Figure 13). The details will be presented under Discussion.

Discussion

The time-resolved SAXS curves obtained from the present PCL/PSO blend have revealed the following two fundamental facts about the process of morphology formation in binary semicompatible crystalline/amorphous blend systems. (1) Blending the amorphous polymer (PSO) retards and stretches the PCL crystallization, but the time dependence of its features, conveniently expressed by the parameters such as long spacing (Figure 5) and

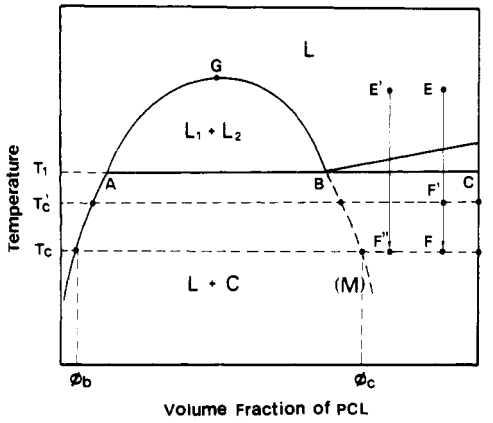

Figure 13. Schematic illustration of the phase diagram with crystallization and liquid–liquid phase separation. L and C denote liquid and perfect crystalline phases, respectively, and the dashed curve represents the lower limit of ϕ_{PCL} in the amorphous layer between PCL lamellae. In the present PCL/PSO system, the critical temperature of phase separation (G) is above 150 °C with the critical composition $\phi_{PCL} \sim 0.2$, and the binodal curve meets with the melting point curve at $\phi_{PCL} \sim 0.58$ and $T_c \sim 54$ °C (B).[21]

intensity maximum (Figures 6 and 7), is substantially the same as those of the crystallization process of the homopolymer (PCL). This indicates that even if the details of the morphology are determined by a cooperative effect of liquid–liquid phase separation and PCL crystallization, the growth rate of the morphology is controlled by the crystallization of PCL in the blend. (2) The details of the morphology are determined by the phase diagram of this system, i.e., a cooperative effect of liquid–liquid phase separation and crystallization. The two-phase structure illustrated in Figure 1 appears at the early stage of morphology formation, and this structure grows with t with the proportion of the amorphous region (and hence the crystalline region) constant. This conclusion comes from the fact that the volume fraction of the amorphous region in the two-phase structure, which is proportional to $\vartheta(t)$ introduced in eq 6, remains constant throughout the morphology formation (Figure 10) but is intimately dependent on ϕ_{PCL} and T_c (Figure 12).

The ϕ_{PCL} and T_c dependences of $\vartheta(t)$ can be qualitatively explained on the basis of the phase diagram exhibiting both crystallization and phase separation. Such a phase diagram has been predicted theoretically[20] and experimentally.[18,19,22,24] Burghardt, for example, calculated the phase diagram of such systems on the basis of the Flory–Huggins theory and discussed the effect of molecular parameters on the equilibrium phase diagram.[20] Figure 13 shows the schematic illustration of the phase diagram constructed in our previous study based on the experimental results.[22] Here, L and C represent the disordered (amorphous) and ordered (perfect crystalline) phases, respectively. In the region denoted $L_1 + L_2$, two disordered phases coexist, and in the region denoted L + C, the disordered phase and perfect crystal of PCL coexist thermodynamically. At temperature T_1, three phases, A, B, and C, coexist thermodynamically (eutectic temperature).[20] In the case of crystallization of polymers, the perfect crystal does not appear; instead, the repeating structure consisting of the lamellar crystal and the amorphous layer always appears. The amorphous layer between lamellae may in part accommodate the PSO expelled from the PCL lamella to result in the increase of the amorphous layer thickness. Therefore, it will be useful to add the third phase M represented by a dashed curve in Figure 13, which stands for the composition of the amorphous phase between lamellae. This third phase is not in thermodynamic equilibrium and may change in composition according to the thermodynamic and kinetic factors in the process of the morphology formation.

When a homogeneous blend at E is quenched into F, $\vartheta(\infty)$ is thermodynamically determined by the lever rule at F if we ignore a small amount of the amorphous component accommodated in the amorphous layers between lamellae, as

$$\vartheta(\infty) \propto (1 - \phi_{PCL})/(1 - \phi_b) \tag{7a}$$

where ϕ_b is the PCL composition of the amorphous region in equilibrium with the perfect PCL crystal and is temperature dependent. This ϕ_b can be evaluated by the equilibrium requirement between chemical potentials of the crystalline and amorphous phases

$$\Delta\mu^L_{PCL} = \Delta\mu^C_{PCL} \tag{8}$$

where C denotes the perfect crystalline phase and L denotes an amorphous phase. By assuming an appropriate model, for example, the Flory–Huggins–Scott model,[32] for the amorphous phase, ϕ_b can be calculated. ϕ_b is, however, expected to be very small. By putting ϕ_b to be 0 to a first approximation, eq 7a is rewritten

$$\vartheta(\infty) \propto 1 - \phi_{PCL} \tag{7b}$$

Equation 7b means that $\vartheta(\infty)$ equals 0 at $\phi_{PCL} = 1$ and increases linearly with decreasing ϕ_{PCL}, which is in good agreement with Figure 12. The proportion of the amorphous region is, therefore, larger when a blend at E′ is quenched into F″ compared to a blend at E quenched into F (at the same temperature T_c). Thus, the initial composition ϕ_{PCL} is expected to dramatically affect the final proportion of the amorphous and crystalline regions in the blend. When the blend at E is quenched into F′, on the other hand, the phase relations at F′ are not so different from those at F; in other words, ϕ_b changes slightly, so that eq 7b holds approximately at different temperatures. The difference in the amount of the amorphous polymer accommodated in the amorphous layer changes principally the final proportion of the amorphous and crystalline regions in the two-phase structure of the blend.

The phase diagram presented in Figure 13 seems to explain the ϕ_{PCL} and T_c dependences of $\vartheta(\infty)$ as well as all SAXS curves exhibiting both the intensity maximum arising from the crystalline region and the increasing intensity at smaller angle. It is necessary to confirm the validity of this kind of phase diagram by the accumulation of many experimental results.

Acknowledgment. This work was supported in part by a grant of the Association for the Progress of New Chemistry (ASPRONC) and has been performed under the approval of the Photon Factory Program Advisory Committee (Proposal 90-061).

References and Notes

(1) Paul, D. R., Newman, S., Eds. *Polymer Blends*; Academic Press: New York, 1978; Vol. 1.
(2) Khambatta, F. B.; Warner, F.; Russell, T. P.; Stein, R. S. *J. Polym. Sci., Polym. Phys. Ed.* **1976**, *14*, 1391.
(3) Stein, R. S.; Khambatta, F. B.; Warner, F. P.; Russell, T. P.; Escala, A.; Balizer, E. *J. Polym. Sci., Polym. Symp.* **1978**, *63*, 313.
(4) Nojima, S.; Tsutsui, H.; Urushihara, M.; Kosaka, W.; Kato, N.; Ashida, T. *Polym. J.* **1986**, *18*, 451.
(5) Morra, B. S.; Stein, R. S. *J. Polym. Sci., Polym. Phys. Ed.* **1982**, *20*, 2243.

(6) Morra, B. S.; Stein, R. S. *J. Polym. Sci., Polym. Phys. Ed.* **1982**, *20*, 2261.
(7) Ito, H.; Russell, T. P.; Wignall, G. D. *Macromolecules* **1987**, *20*, 2213.
(8) Chow, T. S. *Macromolecules* **1990**, *23*, 333.
(9) Elsner, G.; Zachmann, H. G.; Milch, J. R. *Makromol. Chem.* **1981**, *182*, 657.
(10) Russell, T. P.; Koberstein, J. T. *J. Polym. Sci., Polym. Phys. Ed.* **1985**, *23*, 1109.
(11) Schouterden, P.; Riekel, C.; Koch, M.; Groeninckx, G.; Reynaers, H. *Polym. Bull.* **1985**, *13*, 533.
(12) Nojima, S.; Kosaka, W.; Ashida, T.; Muroga, Y.; Ueki, T.; Hiragi, Y.; Kataoka, M.; Izumi, Y.; Tagawa, H.; Amemiya, Y. *Polym. J.* **1985**, *17*, 1229.
(13) Ungar, G.; Keller, A. *Polymer* **1986**, *27*, 1835.
(14) Barham, P. J.; Keller, A. *J. Polym. Sci., Polym. Phys. Ed.* **1989**, *27*, 1029.
(15) Buchner, S.; Wiswe, D.; Zachmann, H. G. *Polymer* **1989**, *30*, 480.
(16) Schouterden, P.; Vandermarliere, M.; Riekel, C.; Koch, M. H. J.; Groeninckx, G.; Reynaers, H. *Macromolecules* **1989**, *22*, 237.
(17) Song, H. H.; Wu, D. Q.; Chu, B.; Satkowski, M.; Ree, M.; Stein, R. S.; Phillips, J. C. *Macromolecules* **1990**, *23*, 2380.
(18) Endres, B.; Garbella, R. W.; Wendorff, J. H. *Colloid Polym. Sci.* **1985**, *263*, 361.
(19) Briber, R. M.; Khoury, F. *Polymer* **1987**, *28*, 38.
(20) Burghardt, W. R. *Macromolecules* **1989**, *22*, 2482.
(21) Nojima, S.; Terashima, Y.; Ashida, T. *Polymer* **1986**, *27*, 1007.
(22) Nojima, S.; Satoh, K.; Ashida, T. *Macromolecules* **1991**, *24*, 942.
(23) Tanaka, H.; Nishi, T. *Phys. Rev. Lett.* **1985**, *55*, 1102.
(24) Tanaka, H.; Nishi, T. *Phys. Rev. A* **1989**, *39*, 783.
(25) Hosemann, R.; Bagchi, S. N. *Direct Analysis of Diffraction by Matter*; North-Holland: Amsterdam, 1962.
(26) Debye, P.; Bueche, A. M. *J. Appl. Phys.* **1949**, *20*, 518.
(27) Elsner, G.; Riekel, C.; Zachmann, G. *Adv. Polym. Sci.* **1985**, *67*, 1. Gehrke, R. *Top. Curr. Chem.* **1989**, *171*, 111.
(28) Ueki, T.; Hiragi, Y.; Kataoka, M.; Inoko, Y.; Amemiya, Y.; Izumi, T.; Tagawa, H.; Muroga, Y. *Biophys. Chem.* **1985**, *23*, 115.
(29) Hashimoto, T. *Phase Transitions* **1987**, *8*, 245.
(30) Glatter, O. *J. Appl. Crystallogr.* **1974**, *7*, 147.
(31) Tsvankin, D. *Polym. Sci. USSR (Engl. Transl.)* **1964**, *6*, 2304.
(32) Scott, R. L. *J. Chem. Phys.* **1949**, *17*, 279.